JOURNAL OF GEOPHYSICAL RESEARCH, VOL. 106, NO. D11, PAGES 11,937–11,956, JUNE 16, 2001

Radiation transfer model intercomparison (RAMI) exercise

Bernard Pinty,[1] Nadine Gobron,[1] Jean-Luc Widlowski,[1] Sigfried A. W. Gerstl,[1] Michel M. Verstraete,[1] Mauro Antunes,[2] Cédric Bacour,[3] Ferran Gascon,[4] Jean-Philippe Gastellu,[4] Narendra Goel,[5] Stéphane Jacquemoud,[3] Peter North,[6] Wenhan Qin,[7] and Richard Thompson[8]

Abstract. The community involved in modeling radiation transfer over terrestrial surfaces designed and implemented the first phase of a radiation transfer model intercomparison (RAMI) exercise. This paper discusses the rationale and motivation for this endeavor, presents the intercomparison protocol as well as the evaluation procedures, and describes the principal results. Participants were asked to simulate the transfer of radiation for a variety of precisely defined terrestrial environments and illumination conditions. These were abstractions of typical terrestrial systems and included both homogeneous and heterogeneous scenes. The differences between the results generated by eight different models, including both one-dimensional and three-dimensional approaches, were then documented and analyzed. RAMI proposed a protocol to quantitatively assess the consequences of the model discrepancies with respect to application, such as those motivating the development of physically based inversion procedures. This first phase of model intercomparison has already proved useful in assessing the ability of the modeling community to generate similar radiation fields despite the large panoply of models that were tested. A detailed analysis of the results also permitted to identify apparent "outliers" and their main deficiencies. Future undertakings in this intercomparison framework must be oriented toward an expansion of RAMI into other and more complex geophysical systems as well as the focusing on actual inverse problems.

1. Introduction

The primary goal of remote sensing research is to establish the existence and nature of the formal relations between the radiative data collected on board of space platforms and the variables of interest for the given applications. These radiative data are controlled by the state variables of the radiation transfer problem, i.e., the smallest set of fundamental quantities required to fully describe the radiation transfer regime in the geophysical media and not exclusively by the variables of interest [e.g., *Verstraete et al*., 1996]. The physical representation of the radiation transfer regime into geophysical media and at its geophysical boundaries is expressed in radiation transfer (RT) models. Any interpretation of satellite data relies on performing the inversion of a model against a data string; models can be conceptual, empirical, or based on the mathematical representation of the physics underpinning radiation transfer as implemented into RT models. RT models therefore constitute an essential component for the quantitative interpretation of remote sensing data and the accuracy and reliability of the solutions to the inverse problems are determined by the performance of both RT models and remote sensing instruments.

In response to scientific questions and recent technological developments, all major Space Agencies have invested sizable resources to design and implement a new generation of Earth Observation platforms and sensors to monitor adequately the land surface properties [e.g., *Diner et al*., 1999]. The upcoming availability of such advanced instruments has, in turn, motivated significant algorithmic development and sophistication which capitalizes on the improvements, made during the last decades by the RT community, in understanding the interaction between the solar radiation and the land surfaces (see, for example, the review papers by *Goel* [1988] and *Pinty and Verstraete* [1997]). Technological advances in aerospace and computer technologies allow the acquisition of data under much better defined observation protocols, and recent theoretical and simulation achievements should permit to take better advantage of these new measurements [see *Verstraete et al*., 2000]. By the same token, the full and proper interpretation of these new data sets will be better assessed to the extent that intrinsic uncertainties of the RT models are evaluated and further decreased. The achievement of this goal requires an assessment of, at least, (1) their relative performances via an intercomparison exercise and (2) their accuracy and reliability in simulating well-documented in situ measurements of RT fields.

This paper describes the purpose and methodology of the radiation transfer model intercomparison (RAMI) exercise

[1]Global Vegetation Monitoring Unit, SAI-EC Joint Research Centre, Ispra, Italy.
[2]Instituto Nacional de Pesquisas Espaciais, Sao Jose dos Campos, São Paulo, Brazil.
[3]Laboratoire Environnement et Développement, Université Paris 7, Paris, France.
[4]Centre d'Etudes Spatiales de la Biosphère, Toulouse, France.
[5]Department of Computer Science, Wayne State University, Detroit, Michigan.
[6]NERC Centre for Ecology and Hydrology, Monks Wood, United Kingdom.
[7]NASA Goddard Space Flight Center, Atmospheric Chemistry and Dynamics, Greenbelt, Maryland.
[8]Alachua Research Institute, Alachua, Florida.

Paper number 2000JD900493.
0148-0227/01/2000JD900493$09.00

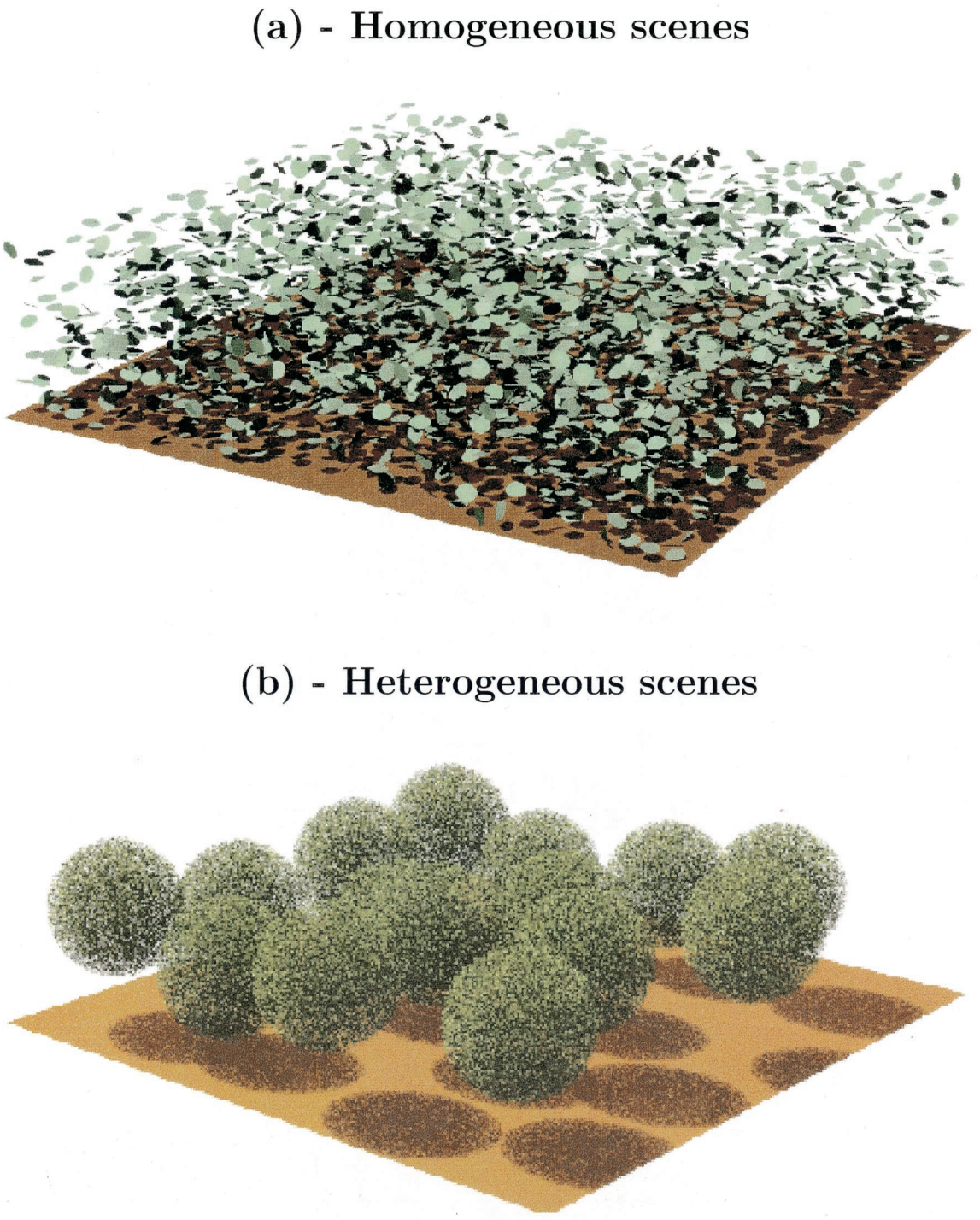

Plate 1. Artist views of the RAMI scenes for discrete (a) homogeneous and (b) heterogeneous scenes.

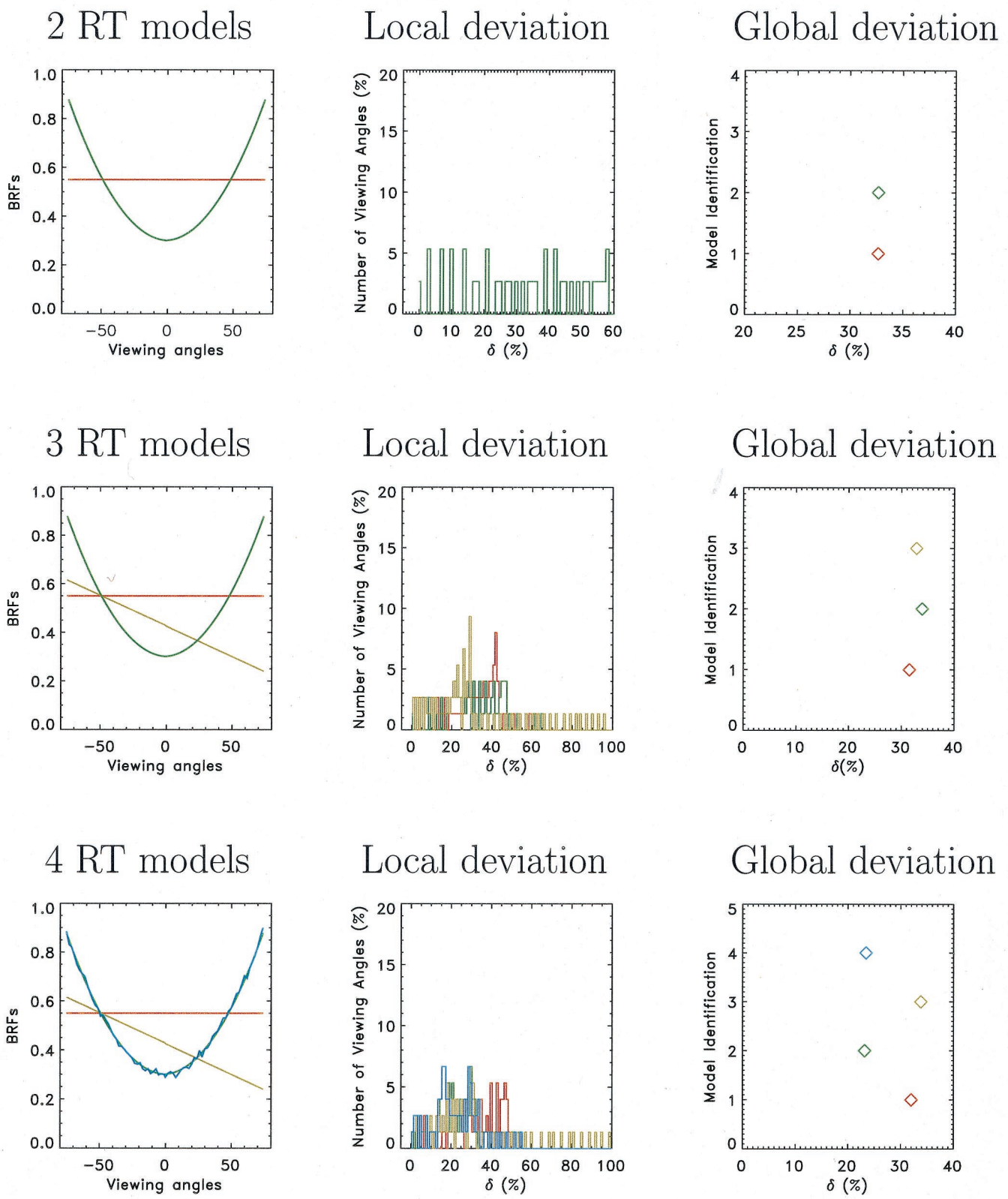

Plate 2. Illustration of the intercomparison strategy concept adopted in the RAMI exercise. The left panels show differences in BRF fields that can be produced by various idealized models, the middle panels give the histograms of the local deviations (in percent) for every model, and the right panels indicate the corresponding values of the global deviation (in percent).

Table 1. List of RAMI Models, References, and Participants

Model Type	Model Name	Reference	Participant
1-D	ProSAIL	*Verhoef* [1984] and *Jacquemoud and Baret* [1990]	C. Bacour[a] and S. Jacquemoud[a]
homogeneous	ProKuusk	*Kuusk* [1995] and *Jacquemoud and Baret* [1990]	C. Bacour and S. Jacquemoud
scenes	1/2 Discrete	*Gobron et al*. [1997]	N. Gobron[b]
3-D	Flight	*North* [1996]	P. North[c]
heterogeneous	DART	*Gastellu-Etchegorry et al*. [1996]	F. Gascon[d] and J.-P. Gastellu[d]
scenes	Sprint	*Thompson and Goel* [1998]	R. Thompson[e] and N. Goel[f]
	RAYTRAN	*Govaerts and Verstraete* [1998]	J.-L. Widlowski[b]
	RGM	*Qin and Gerstl* [1999]	W. Qin[g]

[a]Laboratoire Environnement et Développement.
[b]Joint Research Centre.
[c]Natural Environment Research Council.
[d]Centre d'Etudes Spatiales de la Biosphère.
[e]Alachua Research Institute.
[f]Wayne State University.
[g]Goddard Space Flight Center.

(Historically, the remote sensing community had already performed a "model cook-off" in the mid-1980s when the first computer models were tested for their usefulness in the interpretation of remote sensing data (N. Goel and F. Hall, private communication, 1999.)) and outlines the results achieved so far. This initiative constituted a key part of the preparation for the "Second International Workshop on Multiangular Measurements and Models (IWMMM-2)" held at the Joint Research Centre (JRC) (Ispra, Italy) on September 15–17, 1999, where the results were first presented publicly. This intercomparison has been set up by mid-June 1999 as a self-organized activity of the RT modeling community to which any participants can contribute freely and can also derive its benefits. The aim of RAMI is to focus on the performance of the RT models as an ensemble and to document the current uncertainties/errors among existing models in order to establish a consensus among the surface RT modeling community. Such a model intercomparison exercise also provides, in direct mode, benchmark cases and solutions useful in the development and testing of RT models. In the longer term, it establishes a baseline protocol against which further model improvements and developments can be made. The extended results of this first RAMI phase are available on the World Wide Web at the following address: http://www.enamors.org/. Further exercises and new results will continue to use this site for the foreseeable future.

2. Presentation of the RAMI Exercise

A wide variety of radiation transfer models have been designed and published in the literature over the past decades. These operate at different levels of sophistication and are capable of representing one-dimensional or three-dimensional effects, at quite different computational costs. Not all of these models can easily be implemented in practical applications. At the same time, a sizable majority of users of remote sensing data still use rather empirical tools, such as vegetation indices, in a wide variety of applications. In addition, multiangular measurements are becoming available from space platforms. The full exploitation of these data requires physically based algorithms based on RT models, which are the only tools providing the necessary links between the observed fields and the state variables of the target of interest.

A variety of questions could be envisaged in this context. Is the objective solely to "fit" the observed reflectance field, with the understanding that the physics of RT may or may not be properly represented, or do we also require that the relationship between the state variables of the target of interest and the observed reflectance fields are correctly and accurately described? In this latter case, what source of information could serve as the reference or "truth" against which to evaluate the relative performance of the ensemble of models developed by the community?

To advance along those lines, it was proposed to conduct a formal intercomparison exercise where a representative set of models would be run in strictly defined configurations, to allow the comparison of their results. Specifically, we have suggested a two-pronged approach. First, we have proposed a series of experiments in direct mode, where each model is required to simulate the transfer of radiation in precisely defined geophysical scenes. The second and complementary experiment consists in providing a set of spectral and directional reflectances and to require the models to provide their best estimates as to the nature, structure, and properties of the scenes that could have generated such fields.

The overall objectives of this exercise are thus as follows: (1) to help developers improve their models, (2) to provide a rationale for the acquisition of more or better data, (3) to progressively develop a community consensus on the best ways to simulate the transfer of radiation at and near the Earth's surface, or on the optimal ways to exploit remote sensing data, and (4) to inform the user community on the performance of the various models available.

The following sections describe the experimental protocol in direct mode. Precisely defined scenes containing idealized soils and vegetation canopies are described in such a way that the models available can represent the spectral and directional reflectance fields of these targets, and a well-defined methodology is set up to compare the results as an ensemble. A similar exercise in inverse mode has also been proposed, but very few results have been submitted at the time of writing.

Table 2. Variables Defining the Illumination and Viewing Geometries

Symbol	Variable	Values
θ_0	source zenith angle	20° and 50°
θ_v	view zenith angle	from 0° to 70° in step of 2°
ϕ	relative azimuth angle	0° and 180°

2.1. RAMI Protocol

The RAMI protocol was designed around a limited set of modeling exercises for both homogeneous and heterogeneous geophysical conditions or scenes. These have been selected to represent a broad set of well-defined remote sensing problems for which the solutions can be easily compared. They obviously do not pretend to cover the full range of experiments that would be required to fully document all aspects of model performances. Rather, we focused on a limited but still computationally demanding set of basic cases appropriate to fulfill the initial objectives of RAMI.

For all proposed experiments the participants were encouraged to produce, in addition to the total spectral BRF values, the corresponding contributions due to the uncollided radiation by the leaves, the singly collided by the leaves, the radiation multiply collided by the leaves, and the soil, in both the principal and the cross planes. Additional quantities, including the spectral albedo of the canopy, i.e., the directional hemispheral reflectance, and the absorption of radiation in the vegetation layer were also asked for. In the case of the heterogenous scenes, a set of additional diagnostic parameters were also established to help in understanding the origins of any potential discrepancies between the model results. The full documentation on the experimental protocol for all the proposed simulations can be found at the following World Wide Web address: http://www.enamors.org/. RAMI was conceived as a free exercise to which anybody could contribute and, as an example, any user of a published model could run its own and/or other versions of the same code provided elsewhere. Table 1 lists the RAMI models and the corresponding publication in the peer-reviewed literature documenting these models and, finally, the participant names and affiliations.

2.1.1. Homogeneous scenes. As illustrated in Plate 1a, homogeneous scenes are made up of (1) randomly distributed scatterers with anisotropic scattering functions to be treated as a turbid medium (e.g., oriented point-like scatterers) and (2) randomly distributed finite-size scatterers (e.g., equivalent to leaves) with anisotropic scattering properties. The RT problem to be faced for these homogeneous scenes can be solved either using one-dimensional or three-dimensional models. These series of experiments thus permit us to intercompare the performances of models delivering one-dimensional solutions between themselves and also against those given by the more complex models that solve explicitly the RT equation in the three spatial dimensions.

Table 3. Variables Defining the Structure of Homogeneous Scenes

Variable Identification	Values
Leaf area index (LAI)	3 m^2/m^2
Height of the canopy	2.0 m
Equivalent leaf diameter	infinitely small, 0.1 and 0.2 m
Leaf angle distribution	erectophile and planophile

Table 4. Variables Defining the Spectral Leaf and Soil Properties

Variable Identification	Red Values	Near-Infrared Values
Leaf reflectance[a]	0.0546	0.4957
Leaf transmittance[a]	0.0149	0.4409
Soil albedo[b]	0.1270	0.1590

[a]Using a bi-Lambertian scattering law.
[b]Using a Lambertian scattering law.

Tables 2, 3 and 4 summarize the input values for the illumination and viewing geometries, the architectural variable values, and the spectrally dependent values, respectively, to be used for the proposed simulations.

A variety of combinations of these state variable values have been used to simulate the bidirectional reflectance factor (BRF) fields at red and near-infrared wavelengths which are two spectral regions of importance for land surface remote sensing due to the typical signature of green leaves.

Additional sets of exercises have been proposed to verify model compliance with energy conservation and to benchmark the more complex models against those providing quasi-analytical solutions under particular circumstances. These sets are designed to simulate the radiation transfer regime for homogeneous scenes with conservative scattering conditions. In these cases the scatterer reflectance and transmittance values are both equal to 0.5, and the soil reflectance is equal to 1.0. The additional variables are at fixed values equal to 0.1 m for the leaf diameter, 1.0 m^2/m^2 for the leaf area index, and 1.0 m for the height of the canopy, respectively. Two leaf angle distribution functions, namely erectophile and planophile, are suggested for performing the simulations at three different illumination zenith angles, i.e., 0°, 30°, and 60°.

2.1.2. Heterogeneous scenes. Plate 1b exhibits a representation of the heterogenous scenes made up of randomly distributed spherical envelopes of finite size that contain either finite-size randomly distributed elements or quasi-turbid medium. The experiments were designed for models able to provide solutions to the full three-dimensional radiative transfer problem using a variety of approaches relying on ray-tracing techniques, computer graphics, and three-dimensional space solutions of the RT equation. Each individual scene is composed of a horizontal plane featuring the background soil and

Table 5. Variables Defining the Structure of Heterogeneous Scenes

Variable Identification	Values
Leaf shape	Circular disk of negligible thickness
Leaf diameter	infinitely small and 0.2 m
Leaf area index of a sphere	5 m^2/m^2
Leaf angle distribution	uniform
Number of spheres	15
Sphere radius	10 m
Range of sphere center height	from 11 to 19 m
Fractional sphere area coverage	0.471

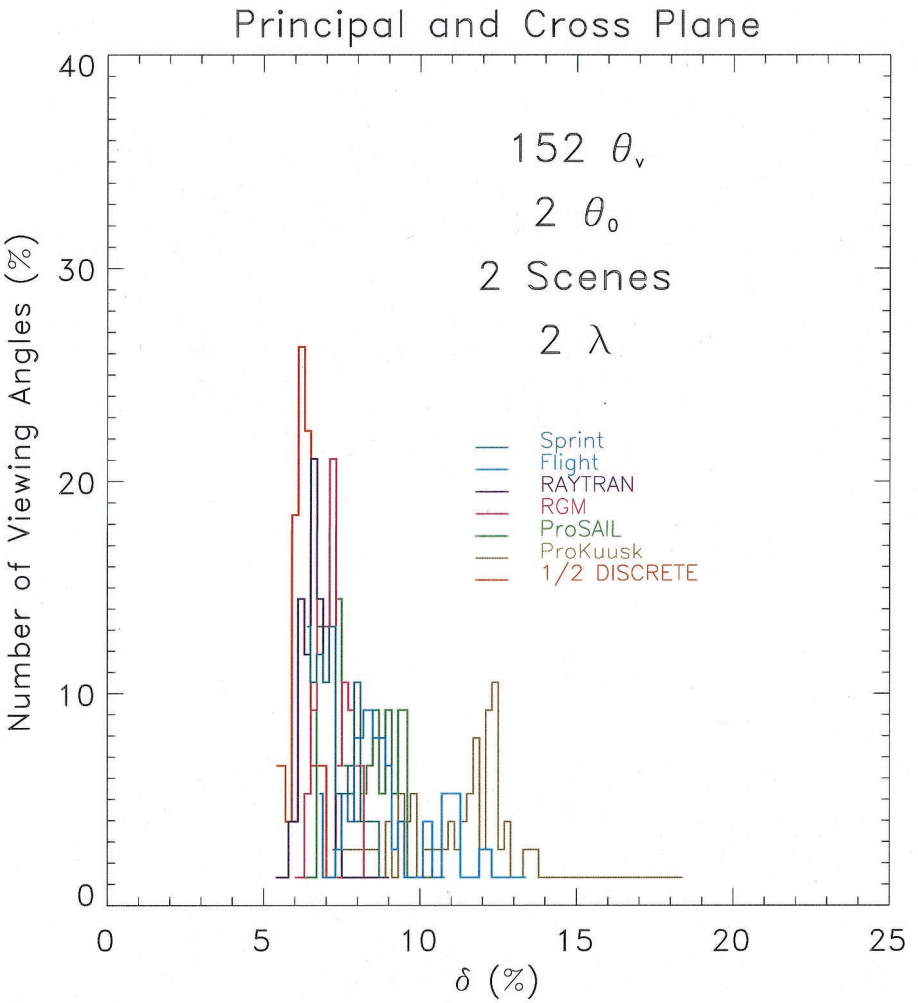

Plate 3. Histogram of the local angular model deviation estimated on the basis of equation (1); that is, values are accumulated over all illumination and viewing geometries and all homogeneous scenes at the red and near-infrared wavelengths.

a number of nonoverlapping disk-shaped scatterers whose normals follow a uniform distribution. The scatterers are confined within large spherical bodies distributed randomly across the scene at various heights. The spectral properties of the individual elements composing the scenes as well as the illumination and viewing conditions are identical to those specified in Tables 4 and 2, respectively. Table 5 provides the values of the key architectural variables specifically used for the scenes.

2.2. Evaluation Strategy

The intercomparison of model results raises a number of fundamental issues and outstanding problems related to the notion of absolute truth and model verification/validation. Such issues have long been debated in all generality by the broad scientific community; an overview of the problems to be addressed in the context of Earth sciences is presented by *Oreskes et al*. [1994]. This contribution provides elements to support the conclusion that the model results cannot be compared against an absolute reference per se which would be the actual "truth" simply because the latter cannot be established. As such, this statement implies that an absolute "model verification" is impossible. Therefore rather than looking for the "truth," the analysis of the ensemble of model results is achieved such that it yields the establishment of the "most credible solutions" as a surrogate for the "truth." Although it is tempting to derive this surrogate from the estimation of the various moments of the distributions of model results, it must be recognized that for instance, model deviations with respect to an ensemble arithmetic average are difficult to interpret in the presence of potential "outliers" that could bias this estimation. Given an ensemble of model results, it is, however, feasible to compare the model results against each other in order to document their relative differences: this is the primary intent of RAMI.

The primary criterion to quantify intermodel variability within the context of RAMI is a measure of distance between BRF fields generated under identical geophysical and geometrical conditions. Specifically, the following metric is computed to estimate how a given model behaves with respect to an ensemble of models:

$$\delta_m(\theta_v) = \frac{1}{\mathcal{N}} \sum_{i=1}^{N_{\theta_0}} \sum_{s=1}^{N_{\text{scenes}}} \sum_{\lambda=1}^{N_\lambda} \sum_{k=1,k\neq m}^{N_{\text{models}}} \frac{|\rho_m(\theta_v, i, s, \lambda) - \rho_k(\theta_v, i, s, \lambda)|}{\rho_m(\theta_v, i, s, \lambda) + \rho_k(\theta_v, i, s, \lambda)} \quad (1)$$

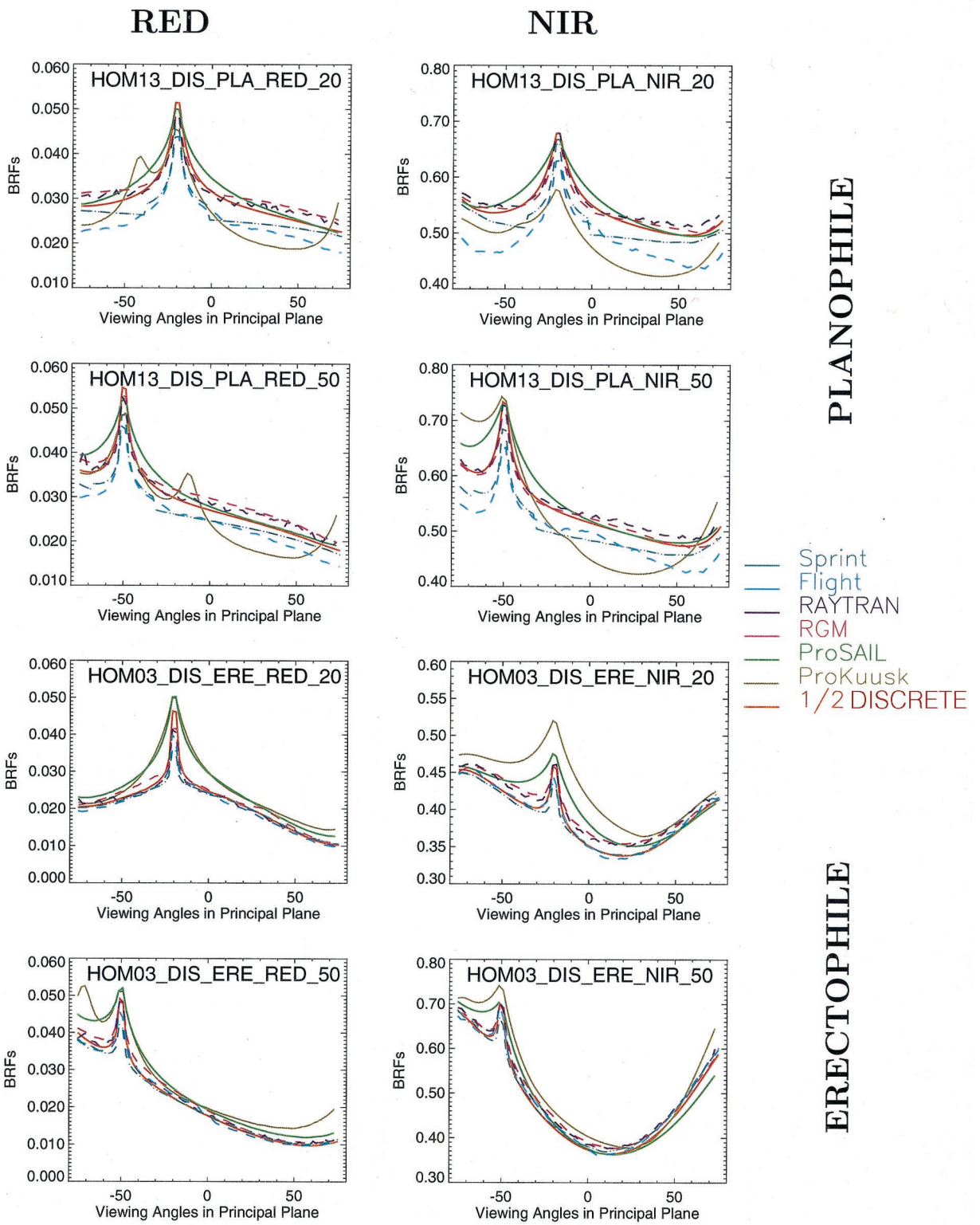

Plate 4. BRF results from the RAMI models plotted in the principal plane for the red (left panels) and near-infrared (right panels) wavelengths, respectively. The four top (bottom) panels correspond to an homogeneous scene specified using a planophile (erectophile) leaf angle distribution function. The conditions of the experiments are given inside each panel using the following convention: DIS stands for discrete medium, PLA (ERE) corresponds to planophile (erectophile) leaf angle distribution, 20 (50) indicates the illumination zenith angle.

where $\delta_m(\theta_v)$ expresses local angular deviation of model m at the specific exiting angle θ_v with respect to the ensemble of N_{models} models. This deviation, normalized by the number of cases considered ($\mathcal{N}$) is estimated for all simulations of the BRF fields, emerging from N_{scenes} at N_λ wavelengths, illuminated with N_{θ_0} incident source angles; $\rho_m(\theta_v, i, s, \lambda)$ and $\rho_k(\theta_v, i, s, \lambda)$ correspond to the BRF values generated by model m and any other RAMI model k participating in the experiment, respectively.

Similar metrics can be designed to examine the model discrepancies for each geometrical condition of illumination and/or observation, scene, and wavelength. They can all be derived following the generic form of (1). For instance, the appropriate metric for analyzing the model discrepancies separately for each wavelength would be

$$\delta_m(\theta_v, \lambda) = \frac{1}{\mathcal{N}} \sum_{i=1}^{N_{\theta_0}} \sum_{s=1}^{N_{\text{scenes}}} \sum_{k=1, k\neq m}^{N_{\text{models}}} \frac{|\rho_m(\theta_v, i, s, \lambda) - \rho_k(\theta_v, i, s, \lambda)|}{\rho_m(\theta_v, i, s, \lambda) + \rho_k(\theta_v, i, s, \lambda)}. \quad (2)$$

Alternatively, (1) can also be ultimately integrated over all available viewing conditions to estimate a global angular model deviation:

$$\delta_m = \frac{1}{N_{\theta_v}} \sum_{l=1}^{N_{\theta_v}} \delta_m(\theta_v), \quad (3)$$

where δ_m denotes a global deviation of the model that results from an estimation of the sum of the local deviations estimated at each and every exiting angle on the basis of the metric expressed by (1).

For the sake of explanation, Plate 2 illustrates the behavior of the measures of the local and global angular deviations in idealized cases. These are based on very simple model results such as those corresponding to a Lambertian medium and perfectly bowl-shaped reflectance fields. This conceptual exercise illustrates that (1) the values of the metrics defined by (1) and (3) depend on the number of RT models entering the intercomparison exercise and (2) the larger the number of models that produce similar BRF fields, the smaller the values estimated by the two metrics. Indeed, the intercomparison of results from two RT models only (top panels) produces rather flat histograms of the local deviation and, obviously, identical global deviation values. The addition of one more model (middle panels), generating BRF fields different from the two former models, draws local deviation values closer to zero but the presence of "outliers" is difficult to assess. In this case, the global deviation metric would slightly favor the Lambertian model (red color) in the sense that it deviates less from the other two. However, when a fourth RT model, generating BRF fields very close to at least one of the former models, is introduced for evaluation (bottom panels), the histograms of the local deviations are significantly narrowed and these similar RT models are more easily identified within the full set on the basis of the global deviation metric by producing lower δ_m values than the others.

In summary, it is worthy to note that as desired in the context of the community effort to assess the state of the art of its models, (1) the larger the number of participating models, the easier the identification of "outliers" if any, (2) the agreement between the BRF fields produced by many models permit identifying them as being able to generate the "most credible solutions."

From the perspective of analyzing the model intercomparison results, it appears that (1) the global deviation metric provides an overall estimation of the model discrepancies, (2) the envelope of the histograms of the local deviation metric values permits to assess the various modes of the distribution of these model discrepancies, and (3) the joint analysis of the individual histograms of the local deviations for every model permits to quantify its behavior against the others. As stated above, any simple statistical analysis tends to favor the subset of models generating the most analogous results. However, in the absence of the absolute "truth," there are no definite reasons to exclude "outliers" on the sole basis of the statistical analyses. An inspection of the physics underlying the RT models and/or the implementation of these models is definitely mandatory to get a rationale regarding model deviations. In practice, the SAI/JRC research group has led the RAMI exercise and has ensured contacts with the participants specifically in case of doubtful results that could have revealed some model implementation errors. This first phase of RAMI was performed blindly by the participants in the sense that they did not know a priori who else was participating, which models were used, and which experiments were made.

3. Overview of RAMI Results

The participants in RAMI performed a large number of radiation transfer computations. These were analyzed and a rather exhaustive set of results is available at the following World Wide Web address: http://www.enamors.org/. This section highlights the most prominent results (The figures and diagrams shown here are built on all results available by end of August 1999.) for the RT modeling and general scientific community.

3.1. Homogeneous Scenes

Figure 1 shows a series of histograms of local angular model deviation values estimated for viewing conditions in the principal plane (left panels), cross plane (middle panels), and the principal and cross planes together (right panels). The top, middle, and bottom panels display the results obtained at the red, the near-infrared, and at the red and near-infrared wavelengths together, respectively. As such, this figure demonstrates the large spread of results delivered by a set of seven BRF models (all models listed in Table 1, but DART, performed the experiments suggested for the homogeneous scenes) representative of the community modeling capacity. Almost all graphs reveal the presence of a first well-marked peak extending from about 8 to 12% and 3 to 6% at the red and near-infrared wavelengths, respectively, and a second peak, less intense close to 15% at the red wavelength. The relative increase in model discrepancies at the red wavelength represents, presumably, the diversity of approaches to address the fundamental plant canopy specific issue of leaf size effects. The values obtained when estimating the local model deviation at the near-infrared wavelength reflects mainly the difference in the methods used to estimate the multiple-scattering components in the plant-soil system.

The panel located at the bottom right of Figure 1 summarizes the values of the local angular deviations when summed up over the two wavelengths and viewing planes. The bimodal

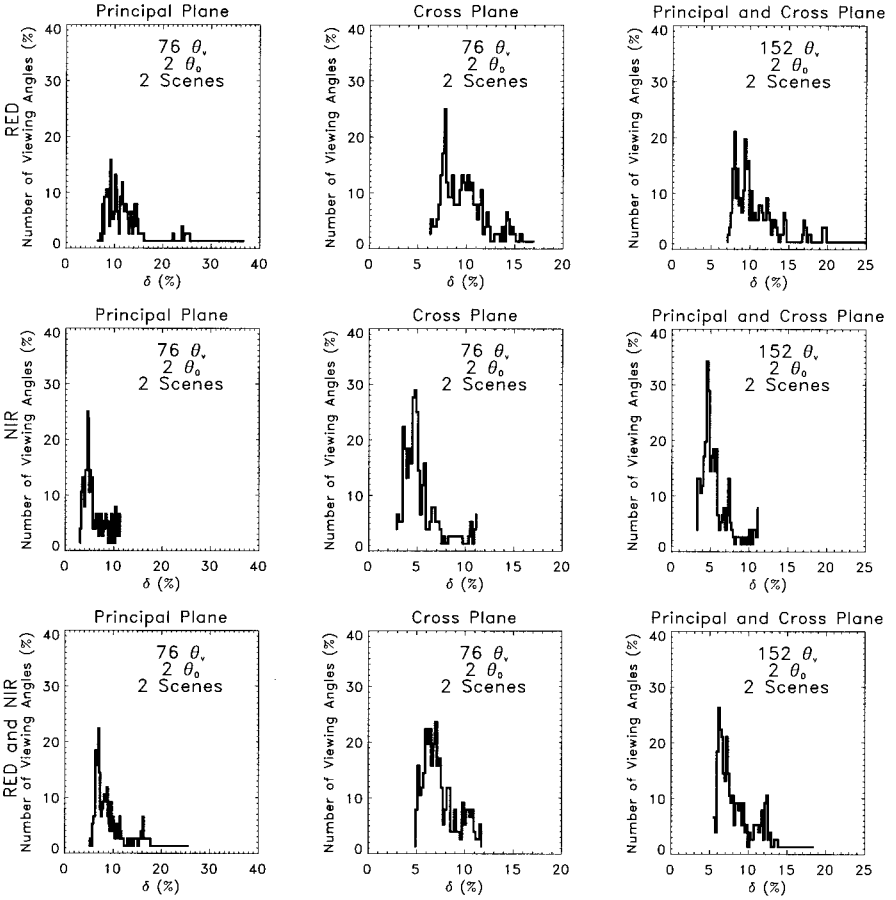

Figure 1. Histograms of local angular model deviations estimated for viewing conditions in the principal plane (left panels), cross plane (middle panels), and the principal and cross planes together (right panels). The top, middle, and bottom panels display the results obtained at red, near-infrared, and red and near-infrared wavelengths together, respectively. All results are obtained using the conditions given in Tables 1, 2, and 3 for the homogeneous scenes.

nature of this histogram indicates the presence of one or more "outliers" in the sense discussed in section 2.1; that is, they produce BRF values that are distinctly different from those delivered by the other RAMI models. A detailed inspection of these results reveal that for all cases examined in Figure 1, two RAMI models are producing the secondary peak. Plate 3 identifies the individual behavior of all RAMI models and reveals that in a statistical sense, both ProKuusk and Flight models deviate the most from the other models.

Plates 4 and 5 exhibit the BRF results delivered by the RAMI models in the principal and cross planes, respectively. Overall, it can be seen that the models show relatively more disagreement between themselves in simulating the planophile canopy conditions. Indeed, in the erectophile case (four bottom panels), only ProKuusk and ProSAIL produce a relatively large backward regime and simulate an angularly larger hot spot than is the case for the other models. The Flight model differs slightly from the other models in generating globally lower BRF values. This difference has been traced to an error in computing the single-scattering phase function, which has since been corrected. Less systematic but still large deviations are produced by ProKuusk in mostly all cases, and additional peaks can be detected both in the principal and in the cross planes outside the hot spot region. The latter are due to the leaf specular reflectance as implemented in the original Kuusk's model. Plates 4 and 5 show clearly that major model discrepancies are occurring in backward conditions and especially within a relatively large solid angle embedding the hot spot effect. It should also be noted, however, that the various implementation of the erectophile and planophile leaf angle distribution functions could have lead to some differences in the model results.

The model discrepancies naturally translate into major angularly integrated quantities such as the absorption and the albedo for direct illumination, i.e., the directional hemispherical reflectance. The results shown in Figures 2 and 3 demonstrate that quite significant variability can be obtained in the case of a planophile leaf angle distribution function. It must be recalled here that the three-dimensional models estimate the integrated quantities in different manners, depending, for instance, on whether they use a direct or inverse Monte Carlo tracing technique.

3.2. Heterogeneous Scenes

Plate 6 shows the histogram of the local angular model deviations estimated by (1), i.e., summed up over the two wavelengths and viewing planes, on the basis of four conceptually different three-dimensional models. It can be seen that the values range from 3 to 6% and that only one model (DART) contributes to the secondary peak at the largest ob-

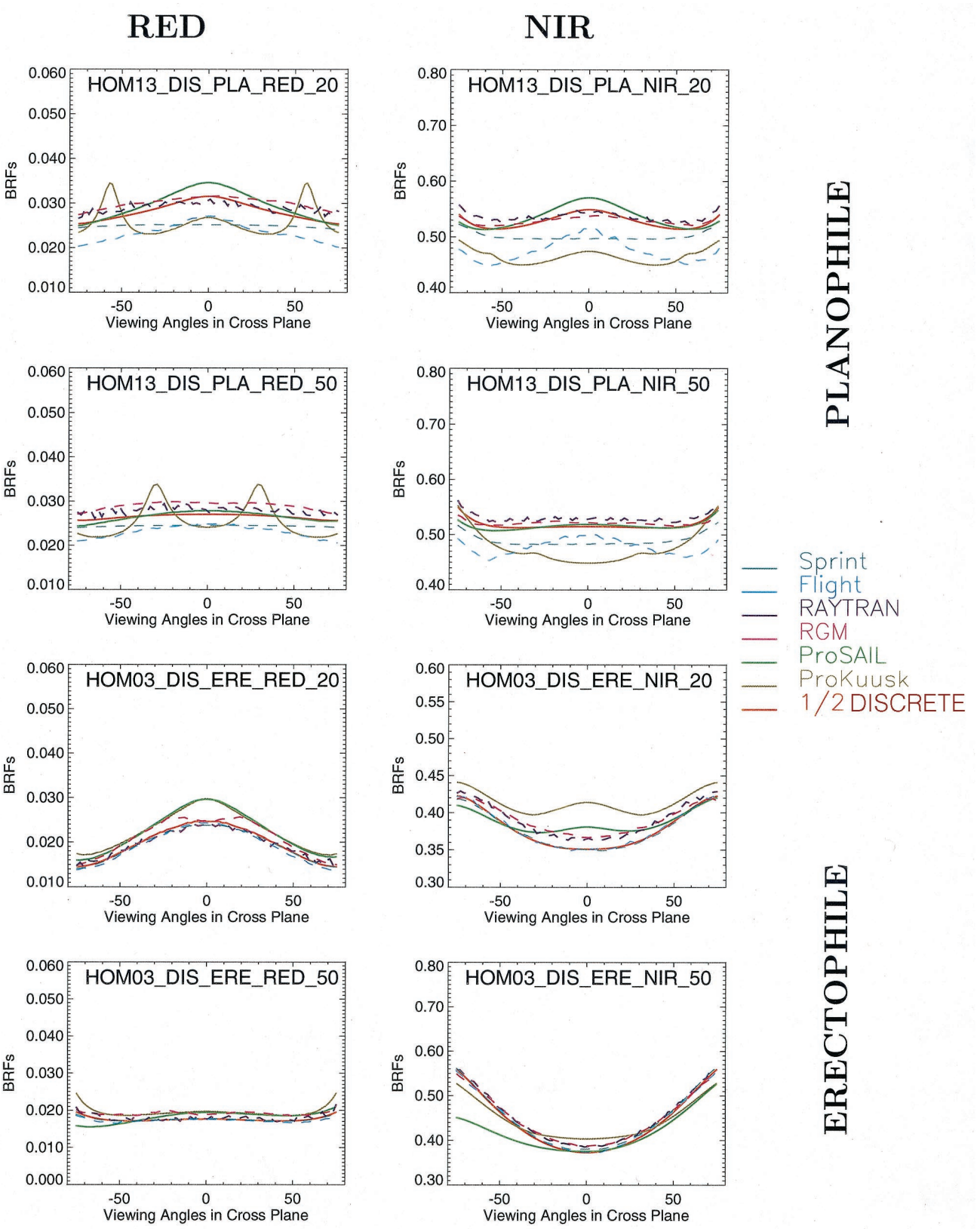

Plate 5. Same as Plate 4 except in the cross plane.

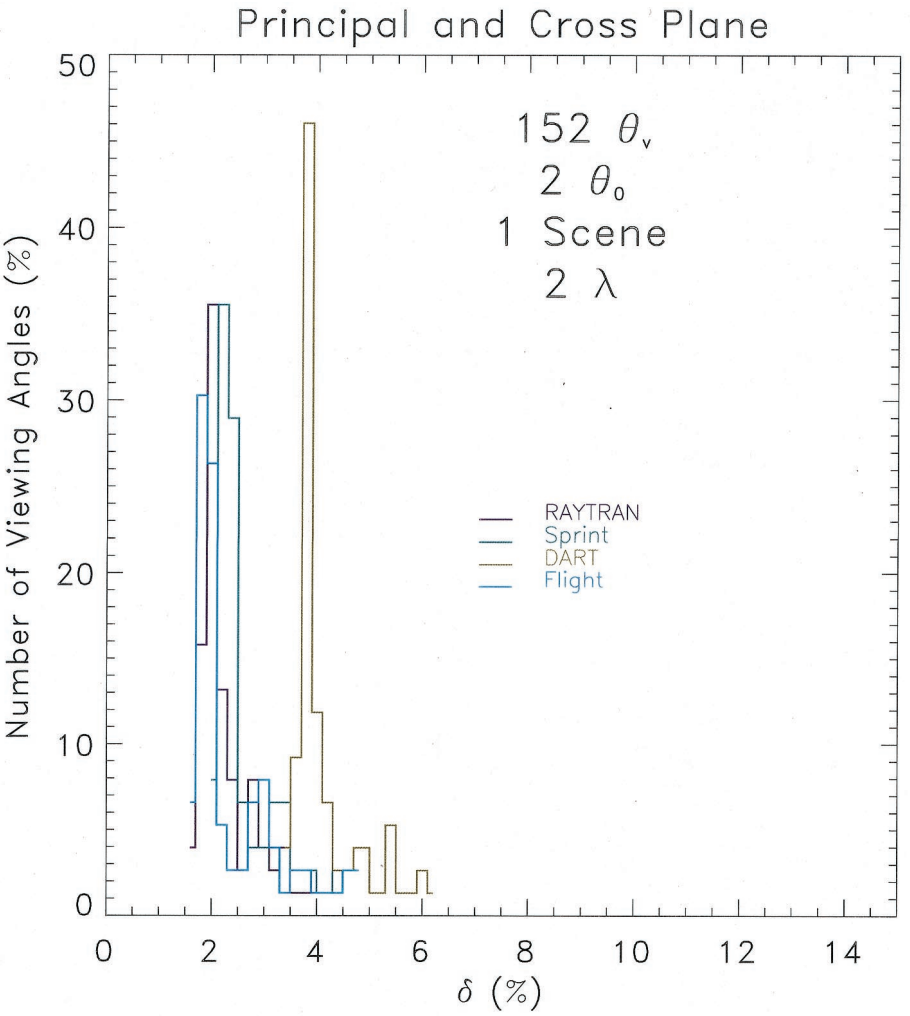

Plate 6. Histogram of the local angular model deviation estimated on the basis of equation (1); that is, values are accumulated over all illumination and viewing geometries and at the red and near-infrared wavelengths for the heterogeneous scenes.

served deviation values. This specific behavior is particularly significant at the near-infrared wavelength and additional results from RAMI show that this is due to a 10% underestimate by DART of the multiple-scattering estimates of the other three models.

Plates 7 and 8 show that indeed for both viewing planes, a good agreement between the three-dimensional models is obtained despite the large dynamic range in the simulated BRF fields. The top four panels of these figures correspond to results obtained in the case of a heterogeneous scene where the spheres are filled up with leaves of 0.2 m diameter producing a well-marked peak in the backscattering region. The bottom panels exhibit BRF fields produced by the same large-scale architecture but for turbid media spheres, i.e., made up of a very large number of point-like oriented (infinitely small) scatterers. In these latter cases the excellent agreement between all three participating models is quite noticeable, in particular, for the representation of the backscattering enhancement controlled by the large-scale voids between the spheres. This is remarkable since the turbid spheres may still be represented by small, yet finite-size scatterers; that is, in the case of RAYTRAN the leaf diameter is equal to 0.002 m.

These slight differences between the three-dimensional model results do not translate into large variations in flux quantities such as the spectral albedo and absorption factors, however, and an overestimate (underestimate) of albedo is mainly compensated by an underestimate (overestimate) of the absorption factor.

3.3. Model Discernability

A well-designed BRF model intercomparison exercise should ideally yield practical indications on the ability of the modeling community to effectively simulate the reflectance fields of a variety of geophysical scenes. This can be done with different tools, provided they represent the same "reality" in numerically acceptable ways. A common issue arising with inverse problems is the occurrence of multiple solutions, i.e., in the present case, the possibility of defining multiple geophysical scenarios that would be able to explain the observations. This situation arises because either there are not enough measurements, or the observations are not accurate enough to constrain the numerical inversion process, or because the models themselves are incorrect or incomplete. In any case this issue becomes one of distinguishing between models that gen-

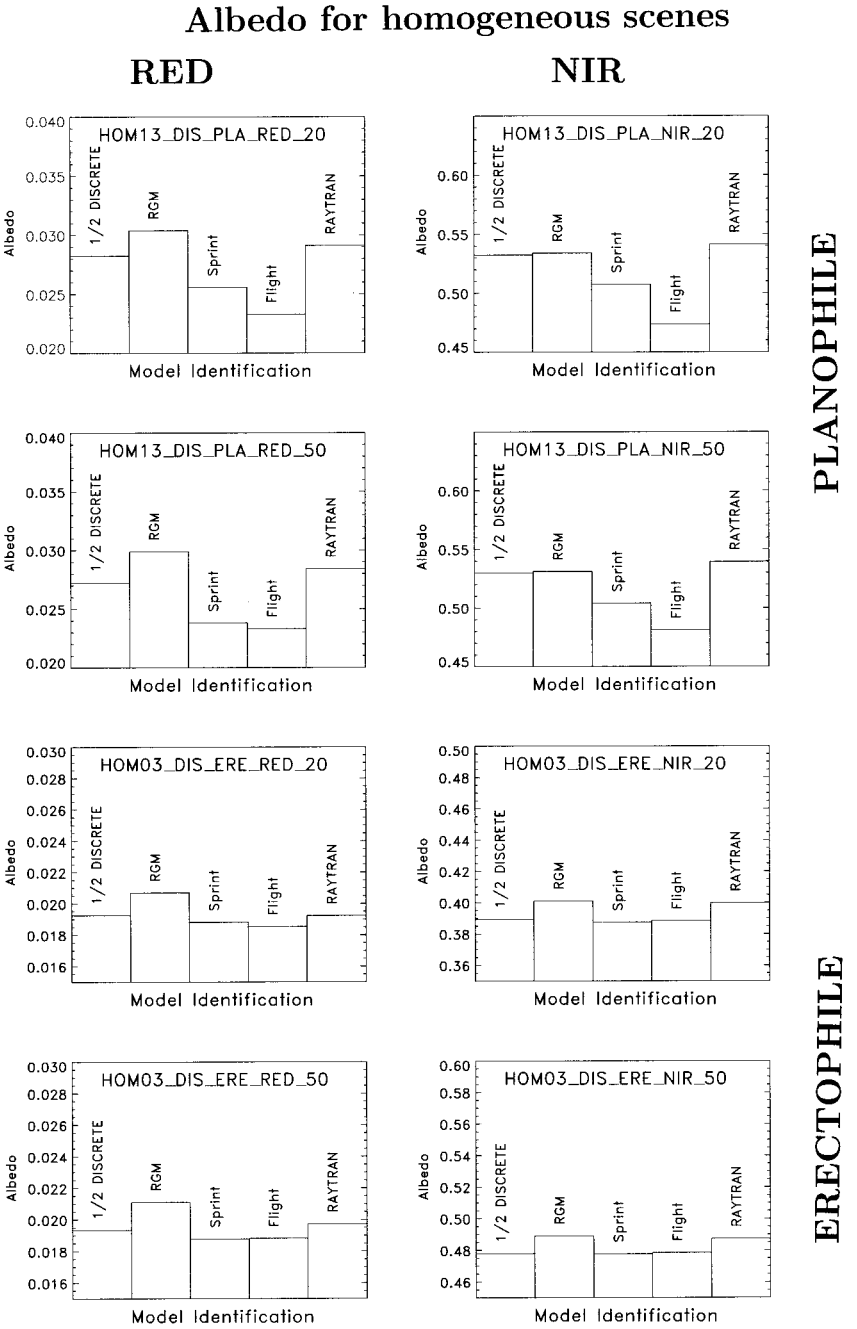

Figure 2. Model results in estimating the spectral albedo, i.e., directional hemispherical reflectance, for the homogeneous scenes at the red (left panels) and near-infrared (right panels) wavelengths. The information provided into each individual panel follows the convention given in Plate 4.

erate different results on the basis of limited samples of imperfect data.

To address this issue, it is necessary to develop an approach where the errors of measurements are somehow compared to the variability exhibited by the different models in their representation of reality. A statistical measure of the joint behavior of these models in terms of their capability of representing a sample of data is thus proposed, and it will be seen that at a given level of accuracy, some models cannot be distinguished, while others can be declared to behave differently. One consequence of this approach is that as measurements improve in accuracy, the differences between models become more noticeable. In a pragmatic sense, differences between RT models matter only to the extent that they exceed the level of uncertainty associated with the measured BRF fields.

The absence of any absolute "truth" in the sense discussed in section 2.2 renders the exercise more tricky, but nevertheless, the model discernability issue can be addressed by assessing the "most credible solutions." As a matter of fact, it can reasonably be admitted that the latter correspond to the actual values that could be measured from an instrument with its intrinsic limited accuracy. We attempted to examine the issue of model discernability taking advantage of the fact that at least in the case of homogeneous scenes, both one-dimensional

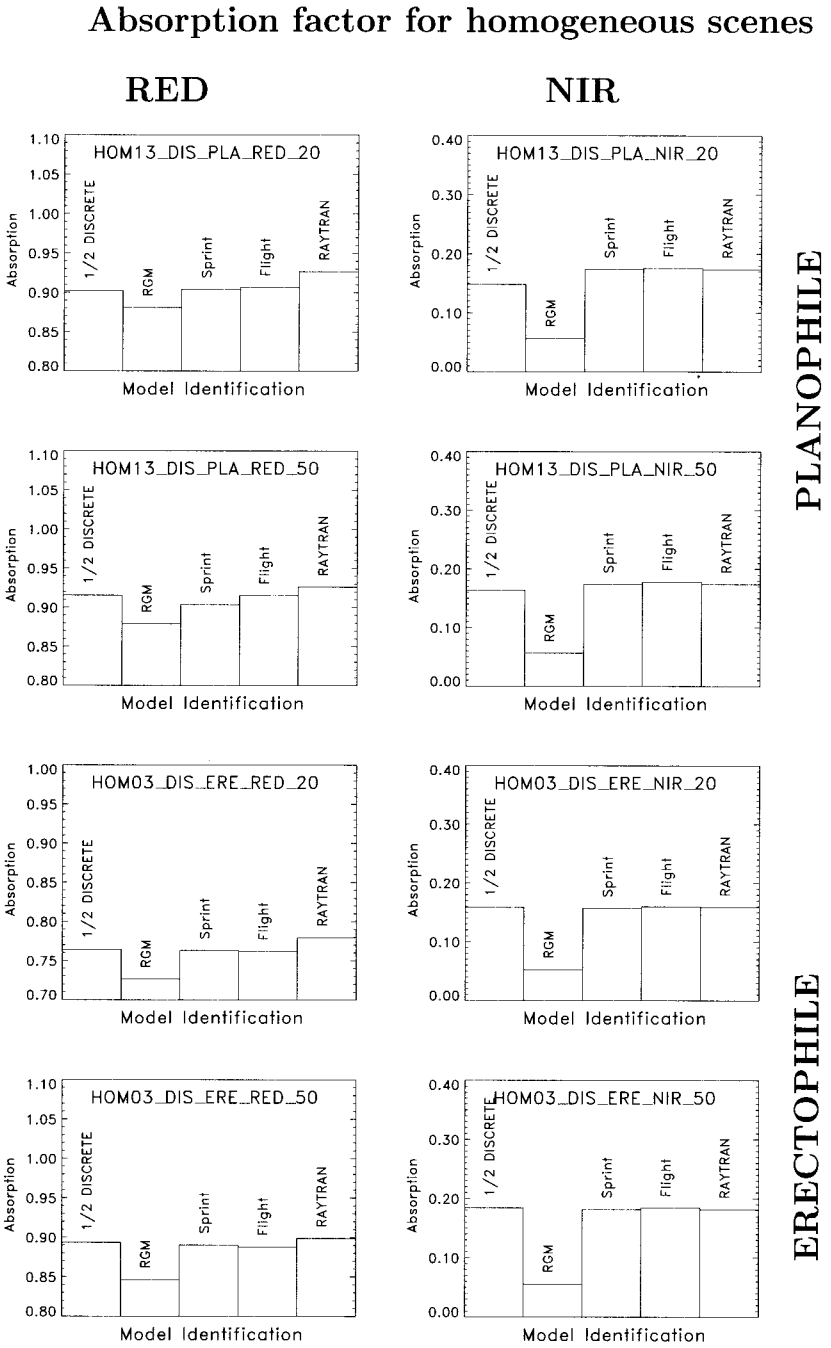

Figure 3. Model results in estimating the spectral absorption factor for the homogeneous scenes at the red (left panels) and near-infrared (right panels) wavelengths. The information provided into each individual panel follows the convention given in Plate 4.

and three-dimensional models could be applied. Accordingly, we established for all scenarios what could be considered as the "most credible solutions" by estimating the arithmetic mean of every BRF value calculated within a subset of the three-dimensional model results. The model discernability can then be analyzed by comparing the values computed with the following normalized χ^2 metric:

$$\chi^2 = \frac{1}{\mathcal{N}} \sum_{i=1}^{N_{\theta_0}} \sum_{j=1}^{N_{\theta_v}} \sum_{s=1}^{N_{\text{scenes}}} \sum_{\lambda=1}^{N_\lambda} \frac{[\rho(i, j, s, \lambda) - \rho^{\text{Credible}}(i, j, s, \lambda)]^2}{\sigma^2(\lambda)}, \tag{4}$$

with

$$\rho^{\text{Credible}}(i, j, s, \lambda) = \langle \rho^{\text{3D}}(i, j, s, \lambda) \rangle, \tag{5}$$

$$\sigma^2_{\text{3D}}(\lambda) = \frac{1}{N_B - 1} \sum_{m=1}^{N_{\text{3D}}} \sum_{i=1}^{N_{\theta_0}} \sum_{j=1}^{N_{\theta_v}} \sum_{s=1}^{N_{\text{scenes}}} [\rho^{\text{3D}}(i, j, s, \lambda) - \rho^{\text{Credible}}(i, j, s, \lambda)]^2. \tag{6}$$

Equations (5) and (6) provide an estimate of the average of the N_B BRF values taken over of a subset of N_{3D} three-

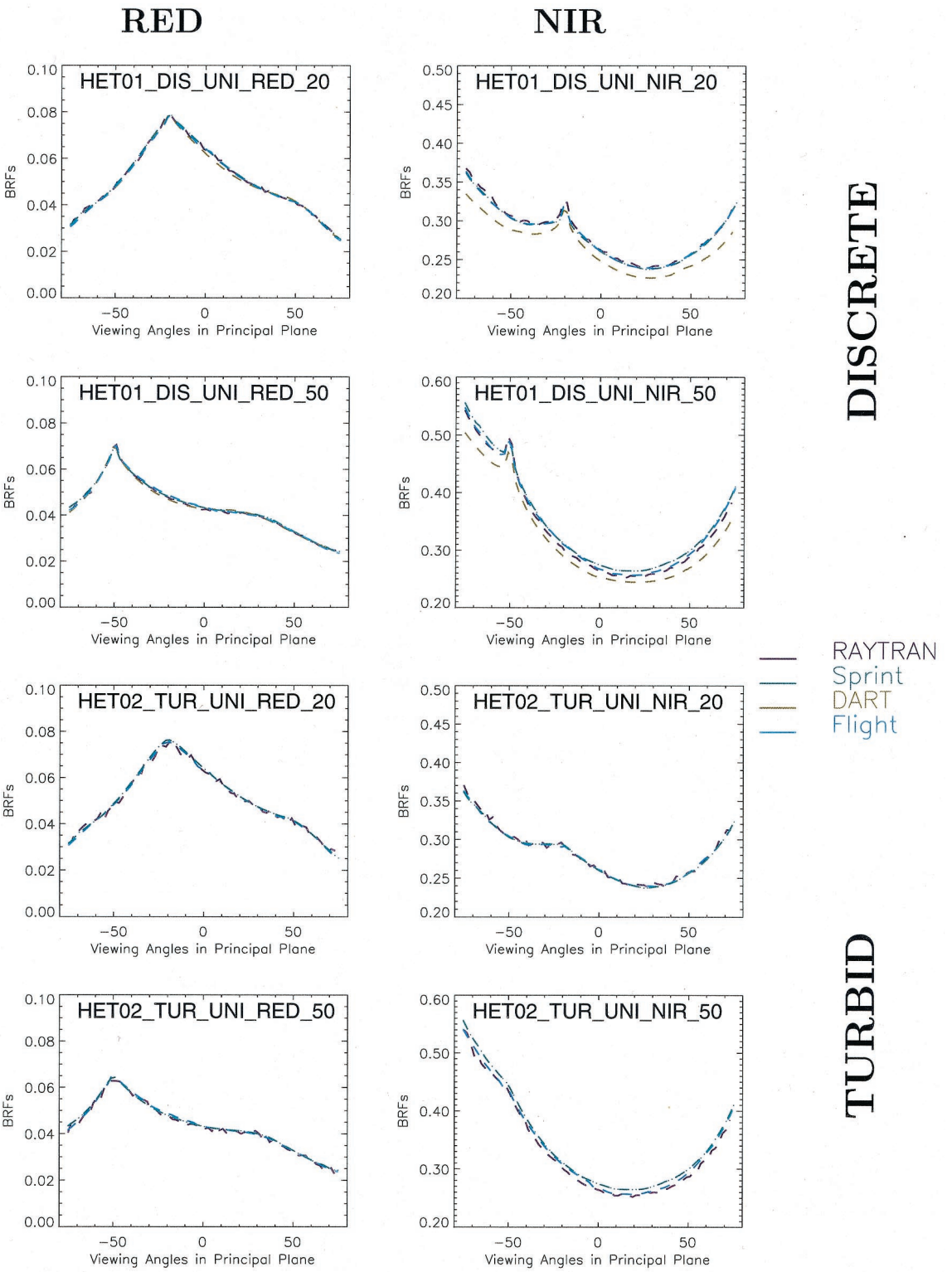

Plate 7. BRF results from the RAMI models plotted in the principal plane for the red (left panels) and near-infrared (right panels) wavelengths, respectively. The four top (bottom) panels correspond to a heterogenous scene specified using a large (extremely small) leaf diameter. The conditions of the experiments are given inside each panel using the following convention: DIS (TUR) stands for discrete (turbid) medium, UNI corresponds to uniform leaf angle distribution, 20 (50) indicates the illumination zenith angle.

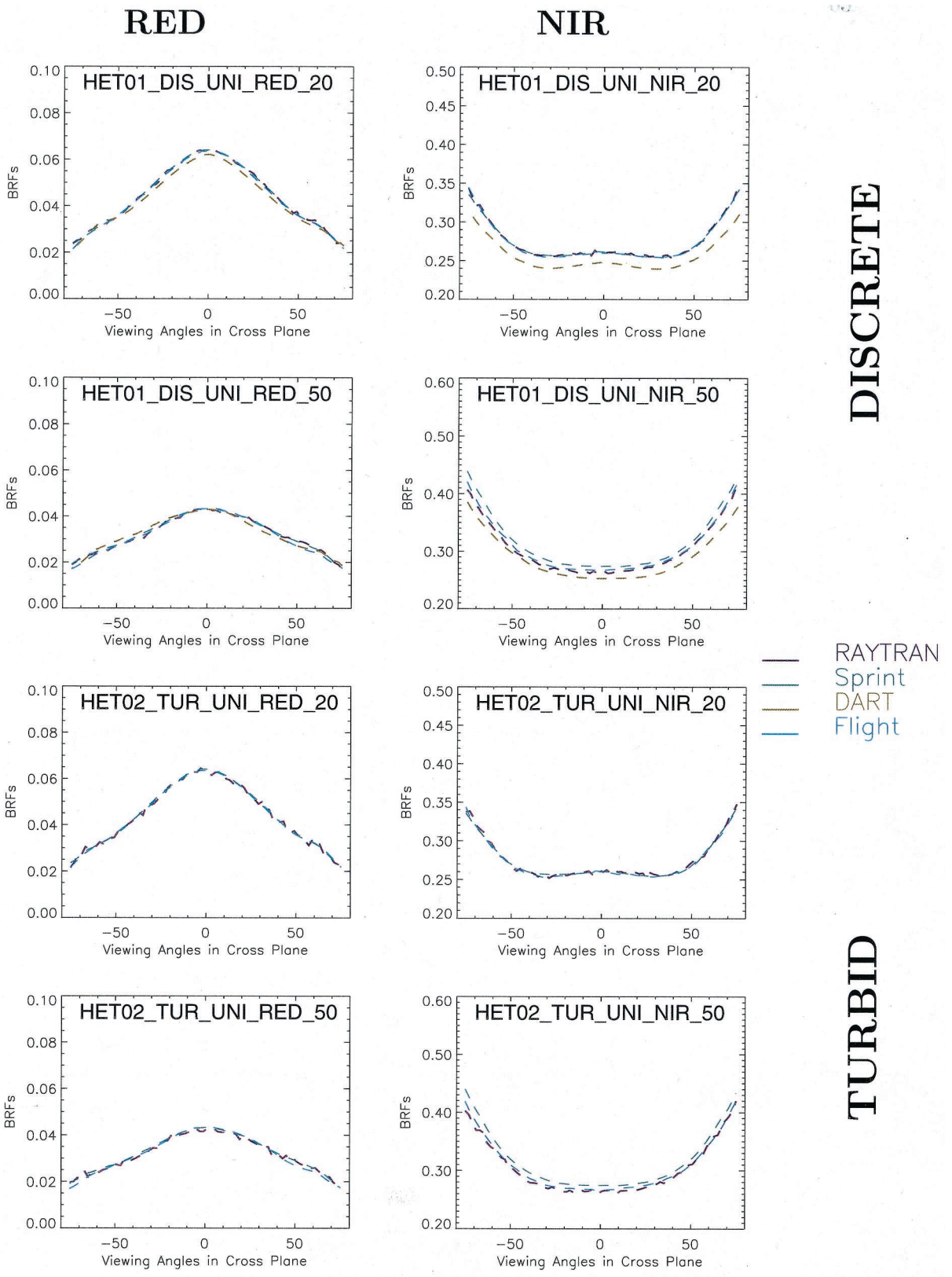

Plate 8. Same as Plate 7 except in the cross plane.

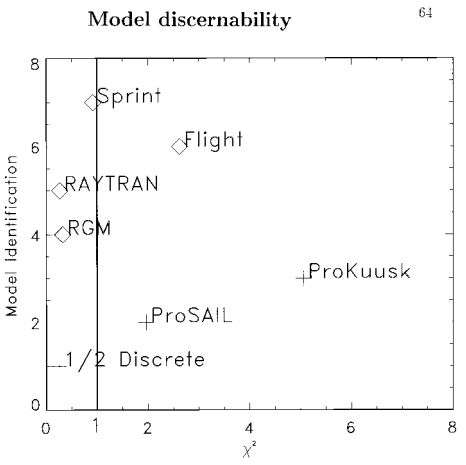

Figure 4. Plots of the χ^2 values estimated using equation (4) for each of the RAMI models in the case of the homogeneous scenes. The cross and diamond signs identify the one-dimensional and three-dimensional models, respectively.

dimensional RAMI models and the associated value of the variance of the BRF distribution of these latter models. $\mathcal{N}$ is a norm equal to the number of available cases. In the present analysis of model discernability we excluded two of the five three-dimensional models that participated in RAMI: the DART and Flight models, which were shown to deviate the most for some of the proposed simulation scenarios. Finally, on the basis of the BRF values generated by the RGM, RAYTRAN, and Sprint models we obtained $\sigma^2_{3D}(\lambda)$ values of 1.6×10^{-3} and 1.0×10^{-2} at the red and near-infrared wavelengths, respectively. These values correspond approximately to 5% and 2% of the typical BRF values that can be measured over a plant canopy system at the red and near-infrared wavelengths, respectively. Such values are within the expected range of those to be estimated from the upcoming multiangular data to be soon gathered in space.

The denominator of (4), $\sigma^2(\lambda)$ corresponds to the sum of the variance associated to each individual model and the actual measurements [*Kahn et al.*, 1997]. As a first attempt, we approximate the value of $\sigma^2(\lambda)$ by simply considering that the uncertainties linked to the models are identical to those associated to the measurements:

$$\sigma^2(\lambda) = 2\sigma^2_{3D}(\lambda). \quad (7)$$

The results of the application of the χ^2 metric defined by (4) are graphically shown in Figure 4. The vertical line at $\chi^2 = 1.0$ defines two subspaces in the diagram. All models falling to the left of this line ($0 < \chi^2 < 1.0$) are indistinguishable on the basis of the available sample of measurements, while those that stand on the right ($\chi^2 > 1.0$) generate BRF fields statistically different at the prescribed level of error. In other words the models located on the left of this line (RAYTRAN, RGM, 1/2 Discrete and Sprint) are simulating BRF fields which are not significantly different, in the sense that the statistical differences between their results cannot be considered meaningful. By contrast, the models Flight, ProSAIL, and ProKuusk do not represent correctly enough the BRF fields from an ensemble of homogeneous scenes. It can readily be foreseen that increasing (decreasing) the data and model accuracies, through the value of the denominator in (4), would move the $\chi^2 = 1.0$ vertical line to the left-hand (right) side of the diagram, so the subset of undiscernable models would become smaller (larger). Hence more accurate data will better help distinguish between models, and their effective interpretation may, in turn, require improved models.

Although this approach remains incomplete, we surmise that this type of RT model intercomparison analysis leads to concrete pragmatic conclusions as far as models are concerned. It also provides sound justification to acquire data with specific accuracy and precision requirements. During this first phase of RAMI, we limited the model discernability analysis to the case of the homogenous scenes because here it is acceptable to define the "most credible solutions" to the radiation transfer problem on the basis of the simulations done by three-dimensional models. The latter showed, however, a good level of agreement in the case of heterogeneous scenes, admitting that some accuracy can easily be gained in the simulation of the multiple-scattering regime by sacrificing more on the computational performances of the code. It is a very encouraging outcome of RAMI that these three-dimensional models are almost equivalent, at least as far as the geophysical scenes we studied are concerned, and this despite the fact that they share very little in terms of approach, numerical methodology and implementation techniques. In the future, better and additional data, or a different set of scenes, may help to assess their limits of applicability, or confirm their correct representation of these measurements.

3.4. Miscellaneous

A number of aspects related to RT modeling have been touched by the RAMI exercise, including information about the computational expenses of the codes, the capacity of addressing a straightforward inverse problem and the verification of model compliance with respect to energy conservation.

The information related to the computational requirements are not reported here since they strongly depend on the coding skills of the programmer and the amount of effort spent in code optimization. In any case, software prototypes can always be tuned to a given platform. Ideally, the intercomparison of model exploitation costs should be conducted under the same computational environment. However, even with these conditions, it will remain difficult to draw definite conclusions on that matter since, as an example, some models may fully profit from specific hardware and software features such as vectorization and parallelization. A dedicated protocol has to be established in order to address the issue of model computational efficiency, as already suggested in the context of the Intercomparison of 3-D Radiation Codes (I3RC) initiative (information about I3RC is available at the following World Wide Web address: http://www.i3rc.gsfc.nasa.gov).

The RAMI initiative also included inverse problems as part of its first phase. We specified two inverse problems where only BRF fields at the top of the canopy were given with the objective of deriving as many biogeophysical parameters of the canopy as possible from an inverse calculation. As in all real-world inverse problems, the solution is not unique because the problem is ill-conditioned. Giving a full or even a partial BRF is equivalent to measuring radiances in different directions above a given scene. Clearly, such data from actual measurements have always uncertainties associated with them which are characteristic of the instrument capabilities and often also contain the effects of atmospheric perturbations that cannot be well defined or corrected for. Consequently, as a first step, we proposed only calculated BRFs without atmospheric effects. In

this case, a specific forward model calculation has been used to produce these BRFs with a particular set of model parameters, so the solution of the inverse problem is known by the research team leading the exercise. This set of model parameter values constitutes the "true solution" of the problem. The inverse problem therefore consists in finding one or more sets of variable values yielding BRF fields not statistically different from the "true" one with respect to the specified uncertainty. The "true solution" can thus be used as a standard for comparing the results from the inverse calculations performed by the intercomparison participants. An additional exercise was defined with the provision of only nine BRF values along a slice through the full BRF distribution at red and near-infrared wavelengths; this more realistic case is taken to be somewhat analogous to the situation that arises for measurements from the MISR instrument on the EOS-Terra platform. Although the specification of these inverse problems offered quite a range of possibilities for many participants (that is, classical vegetation indices can be applied as usually done with actual imperfect data from space), the inverse mode received very little attention and only one participant (F. Gao (Boston University) applied its knowledge-based uncertainty inversion technique.) outside the leading team at JRC did propose some answers. Accordingly, these exercises in inverse mode are still ongoing and should deserve more attention in the future.

The verification of model compliance with respect to energy conservation was addressed on the basis of a set of conservative scattering experiments, as explained in section 2.1. The large computing time requested by some three-dimensional models has been an issue to ensure the performance of these simulations using advanced tools. As a matter of fact, only three models, namely Flight, RAYTRAN, and 1/2 Discrete, have been tested against these academic conditions referring to finite-size scatterers. (Similar experiments were carried out for turbid conditions in which Sprint also participated.) Plates 9 and 10 illustrate the BRF fields simulated by these models in the principal plane for erectophile and planophile leaf angle distribution functions, respectively. The overall agreement between the three model results, especially when considering an erectophile leaf angle distribution function and the lowest leaf area index values, is quite impressive under such drastic scattering conditions. The differences in the simulated BRF results increase almost systematically in the forward scattering direction.

Having set up a pure conservative scattering experiment for homogeneous media made up of finite-size-oriented scatterers, the theoretical albedo and absorption factor values are equal to 1.0 and 0.0, respectively. In all experiments, except in the case of planophile canopy illuminated at 60° for which the simulation results are not available, the RAYTRAN model recovers the theoretical values with a numerical accuracy of about 10^{-4}. The 1/2 Discrete model delivers albedo and absorption factor values which are off by 0.02 (0.045) absolute in the worst case using an erectophile (planophile) leaf angle distribution. These estimates are not available for other models, and statistics can therefore not be established at this time, however, under standard scattering canopy conditions when measured at the red and near-infrared wavelengths, the compliance with respect to energy conservation should be satisfied to a much higher degree of accuracy than with respect to other processes at work.

4. Conclusions and Perspectives

The modeling groups participating in the first phase of the RAMI exercise constitute a significant fraction of the international community, and their models are representative of the range of existing radiation transfer models currently applied in direct and inverse mode. The RAMI initiative is set up as a self-organized and ongoing activity to which any researcher is free to participate. This approach yields a documentation of the variability produced by the models currently in use in the RT modeling community. The first phase has already proved useful in (1) quantifying the variability of BRFs simulated by a large set of RT models under various geophysical scenarios, (2) pointing out some model discrepancies at large angles and in the angular region where backscattering is enhanced by the leaf size effects, (3) benchmarking three-dimensional model simulations and verifying their numerical implementation, and (4) evaluating model discrepancies on the basis of a discernability concept in line with the use of these RT models in an inverse mode.

The overall impression left by inspecting the various results is that the modeling community has reached a high level of maturity because of its willingness to participate in such an exercise. Discrepancies are documented and linked to specific requirements that can be translated into measurement requirements. There are obviously a few specific areas where model improvements can be envisaged and certainly performed without facing significant difficulties. As a matter of fact, some model improvements have already been made by the participants following the evaluation of the results obtained during the first phase of RAMI; an update of the improved model results will be presented during the second phase of the RAMI exercise where it is expected that the model variability in the angular domain will be reduced, at least for these specific cases. The full potential of this intercomparison exercise remains, however, to be exploited through a continuation of this first RAMI phase. It is, for instance, important to have all participating models to perform all experiments in order to make a more complete assessment of their relative capabilities.

With the benefit of the model intercomparison results obtained over simple geophysical scenarios, it can now be envisaged to pursue this strategy by reinforcing the number and variety of canopy conditions to be simulated. For instance, the monitoring and characterization of the boreal and, more specifically, coniferous forests are of major importance for global and regional climate modeling. However, none of the RAMI experiments proposed in this first phase could actually cope with these biome types although some advanced and dedicated models have long been developed [e.g., *Li and Strahler*, 1986; *Li and Strahler*, 1992; *Peltoniemi*, 1993; *Li et al*., 1995; *Knyazikhin et al*., 1997; *Chen and Leblanc*, 1997; *Ni et al*., 1998].

The RAMI results constitute a unique set of simulated BRF fields and a platform against which the improvements from new models, further model developments, and innovation could be objectively assessed. We believe that this platform will stimulate scientific interactions and inform the community on the state of the art at regular time interval. At the same time, we expect that these developments will both justify a posteriori the investments already made to acquire more and better data with laboratory, field, airborne and spaceborne instruments, and motivate the community to pursue further improvements in this direction.

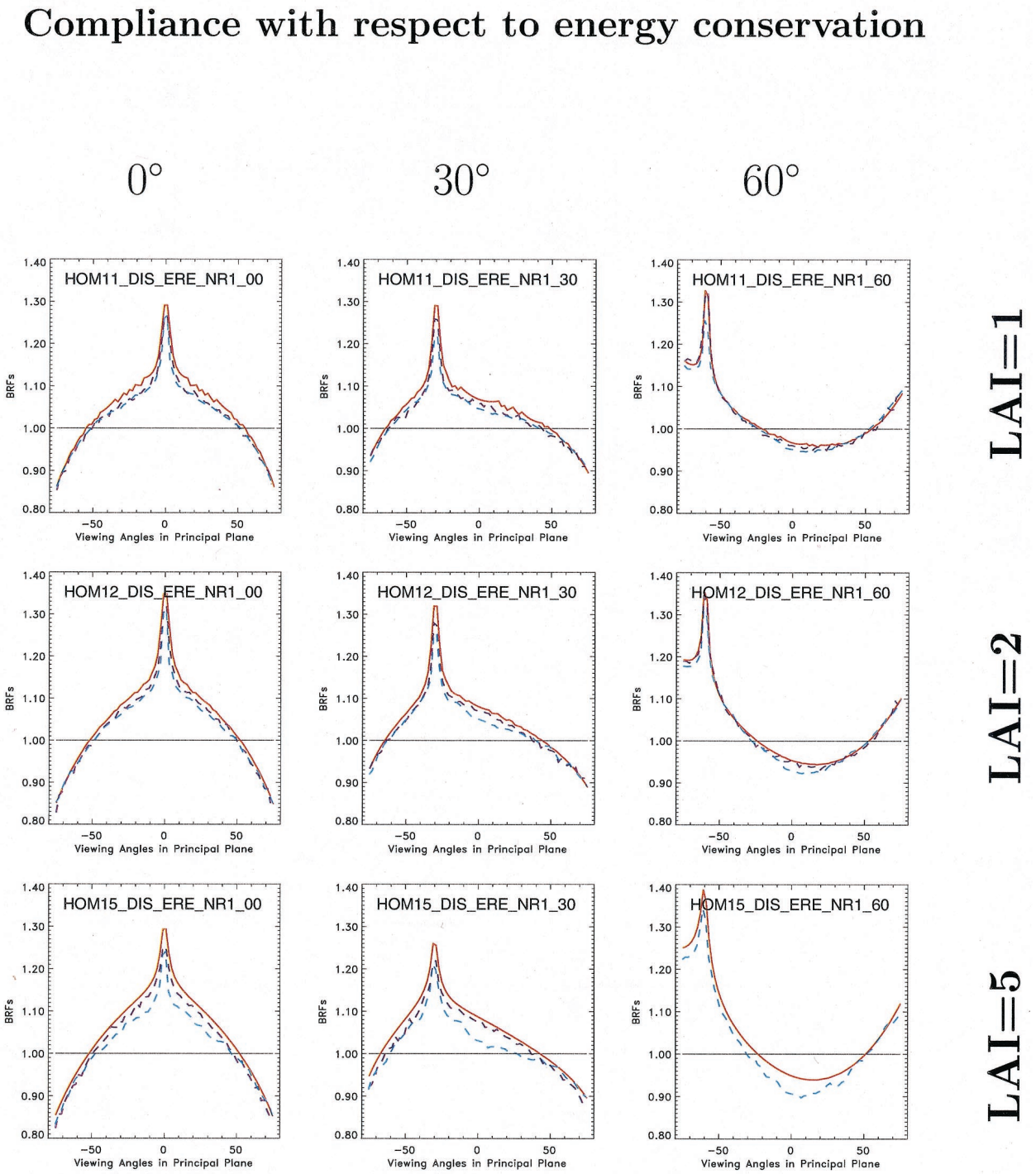

Plate 9. Plots of the BRFs simulated by the Flight (light blue curve), RAYTRAN (deep blue curve), and 1/2 Discrete (red curve) models, in the principal plane for a homogeneous scene with an erectophile leaf angle distribution function. Other variable values are given in section 2.1.

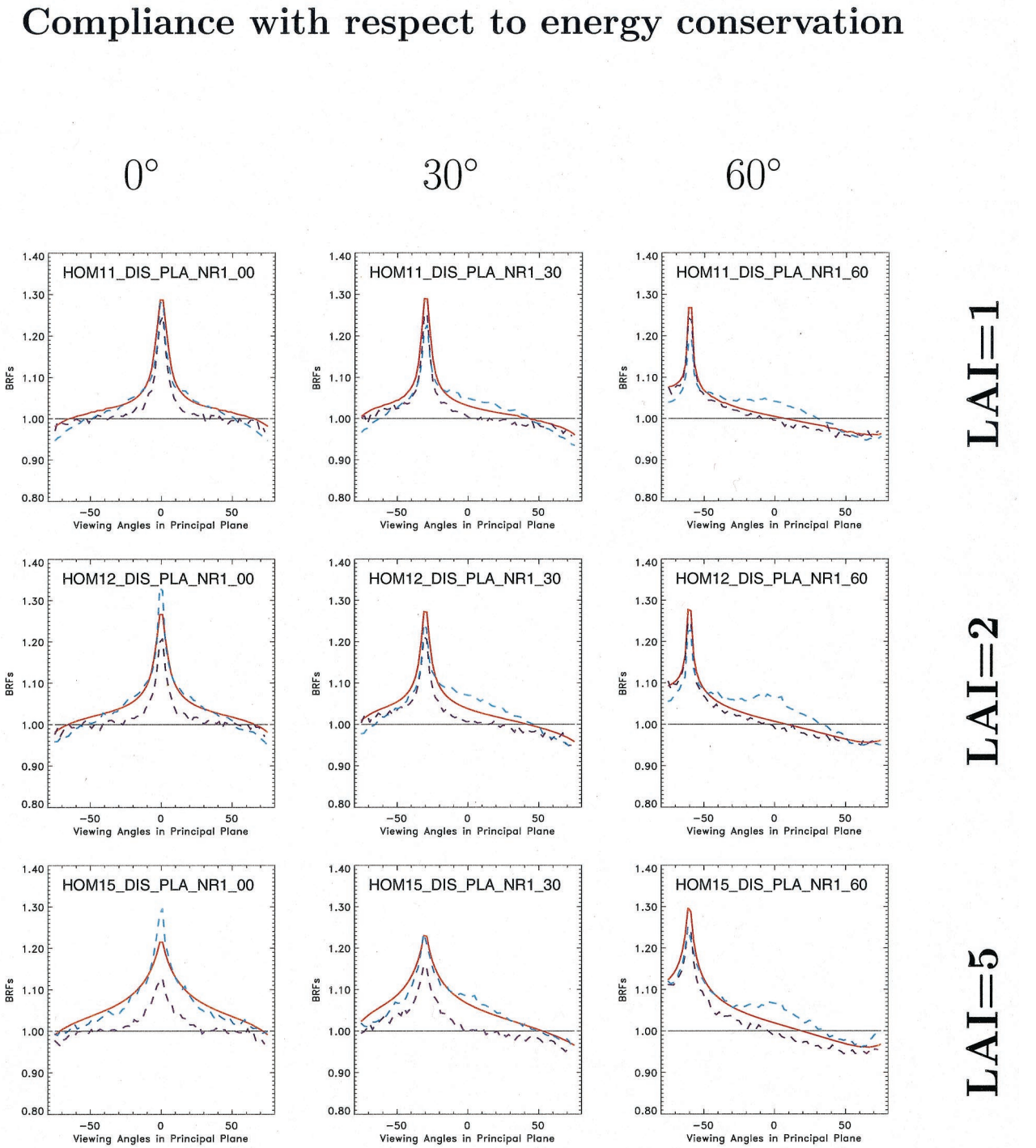

Plate 10. Same as Plate 9 except for a planophile leaf angle distribution function.

Acknowledgments. The technical assistance of Gianni Napoli is gratefully acknowledged by the participants. The RAMI exercise was conceived and implemented as part of the preparation for the IWMMM-2 conference jointly sponsored by (1) the European Network for the development of Advanced Models to interpret Optical Remote Sensing (ENAMORS) data over terrestrial environments supported by the DGXII under the Fourth Framework Programme, (2) the Space Applications Institute (SAI) of the JRC, (3) the National Aeronautics and Space Administration (NASA), and (4) the Commonwealth Scientific and Industrial Research Organization (CSIRO). This paper benefited indirectly from progress achieved by other research groups in geophysics which organized analogous intercomparison exercises in the field of clouds and, more generally, atmospheric models. Mauro Antunes is supported by FAPESP. Many thanks to A. Kuusk who sent C. Bacour and S. Jacquemoud the software code of his Markov chain model of canopy reflectance.

References

Chen, J. M., and S. G. Leblanc, A four-scale bidirectional reflectance model based on canopy architecture, *IEEE Trans. Geosci. Remote Sens.*, *35*, 1316–1337, 1997.

Diner, D. J., G. P. Asner, R. Davies, Y. Knyazikhin, J.-P. Muller, A. W. Nolin, B. Pinty, C. B. Schaaf, and J. Stroeve, New directions in earth observing: Scientific applications of multiangle remote sensing, *Bull. Am. Meteorol. Soc*., *80*, 2209–2228, 1999.

Gastellu-Etchegorry, J.-P., V. Demarez, V. Pinel, and F. Zagolski, Modeling radiative transfer in heterogeneous 3-d vegetation canopies, *Remote Sens. Environ*., *58*, 131–156, 1996.

Gobron, N., B. Pinty, M. M. Verstraete, and Y. Govaerts, A semidiscrete model for the scattering of light by vegetation, *J. Geophys. Res*., *102*, 9431–9446, 1997.

Goel, N., Models of vegetation canopy reflectance and their use in estimation of biophysical parameters from reflectance data, *Remote Sens. Rev*., *4*, 1–212, 1988.

Govaerts, Y., and M. M. Verstraete, Raytran: A Monte Carlo ray tracing model to compute light scattering in three-dimensional heterogeneous media, *IEEE Trans. Geosci. Remote Sens*., *36*, 493–505, 1998.

Jacquemoud, S., and F. Baret, PROSPECT: A model of leaf optical properties spectra, *Remote Sens. Environ*., *34*, 75–91, 1990.

Kahn, R., R. West, D. McDonald, and B. Rheingans, Sensitivity of multiangle remote sensing observations to aerosol sphericity, *J. Geophys. Res*., *102*, 16,861–16,870, 1997.

Knyazikhin, Y. V., G. Miessen, O. Panfyorov, and G. Gravenhorst, Small-scale study of three-dimensional distribution of photosynthetically active radiation in a forest, *Agric. For. Meteorol*., *88*, 215–239, 1997.

Kuusk, A., A Markov chain model of canopy reflectance, *Agric. For. Meteorol*., *76*, 221–236, 1995.

Li, X., and A. H. Strahler, Geometric-optical bidirectional reflectance modeling of a conifer forest canopy, *IEEE Trans. Geosci. Remote Sens*., *24*, 906–919, 1986.

Li, X., and A. H. Strahler, Geometric-optical bidirectional reflectance modeling of the discrete crown vegetation canopy: Effect of crown shape and mutual shadowing, *IEEE Trans. Geosci. Remote Sens*., *30*, 276–292, 1992.

Li, X., A. H. Strahler, and C. E. Woodcock, A hybrid geometric optical radiative transfer approach for modeling albedo and directional reflectance of discontinuous canopies, *IEEE Trans. Geosci. Remote Sens*., *33*, 466–480, 1995.

Ni, W., X. Li, C. E. Woodcock, M. R. Caetano, and A. Strahler, An analytical hybrid gort bidirectional reflectance model for discontinuous plant canopies, *IEEE Trans. Geosci. Remote Sens*., *37*, 987–999, 1998.

North, P. R. J., Three-dimensional forest light interaction model using a Monte Carlo method, *IEEE Trans. Geosci. Remote Sens*., *34*, 946–956, 1996.

Oreskes, N., K. Shrader-Frechette, and K. Belitz, Verification, validation, and confirmation of numerical models in the earth sciences, *Science*, *263*, 641–646, 1994.

Peltoniemi, J., Radiative transfer in stochastically inhomogeneous media, *J. Quant. Spectrosc. Radiat. Transfer*, *50*, 655–671, 1993.

Pinty, B., and M. M. Verstraete, Modeling the scattering of light by vegetation in optical remote sensing, *J. Atmos. Sci*., *55*, 137–150, 1997.

Qin, W., and S. A. W. Gerstl, 3-D scene modeling of semidesert vegetation cover and its radiation regime, *Remote Sens. Environ*., *74*, 145–162, 2000.

Thompson, R. L., and N. S. Goel, Two models for rapidly calculating bidirectional reflectance: Photon spread (ps) model and statistical photon spread (sps) model, *Remote Sens. Rev*., *16*, 157–207, 1998.

Verhoef, W., Light scattering by leaf layers with application to canopy reflectance modeling: The SAIL model, *Remote Sens. Environ*., *16*, 125–141, 1984.

Verstraete, M. M., B. Pinty, and R. B. Myneni, Potential and limitations of information extraction on the terrestrial biosphere from satellite remote sensing, *Remote Sens. Environ*., *58*, 201–214, 1996.

Verstraete, M. M., M. Menenti, and J. Peltoniemi, *Observing Land From Space: Science, Customers and Technology*, Kluwer Acad., Norwell, Mass., 2000.

M. Antunes, Instituto Nacional de Pesquisas Espaciais, Avenida dos Astronaustas 1758, Sao Jose dos Campos, SP, Brazil.

C. Bacour and S. Jacquemoud, Laboratoire Environnement et Développement, Université Paris 7, Denis Diderot, Case Postale 7071, 2, Place Jussieu 75251 Paris, France.

F. Gascon and J.-P. Gastellu, Centre d'Etudes Spatiales de la Biosphère, 18, Avenue Edouard Belin, 31055 Toulouse, France.

S. A. W. Gerstl, N. Gobron, B. Pinty, M. M. Verstraete, and J.-L. Widlowski, Global Vegetation Monitoring Unit, SAI-EC Joint Research Centre, TP 440, via E. Fermi, 21020 Ispra (VA), Italy. (bernard.pinty@jrc.it)

N. Goel, Wayne State University, 431 State Hall, Detroit, MI 48202.

P. North, NERC Centre for Ecology and Hydrology ITE Monks Wood, Cambs PE28 2LS, UK.

W. Qin, NASA Goddard Space Flight Center, Atmospheric Chemistry and Dynamics, Code 916, Greenbelt, MD 20771.

R. Thompson, Alachua Research Institute, 8202 NW 156 Avenue, P.O. Box 1920, Alachua, FL 32616.

(Received March 29, 2000; revised August 3, 2000;
accepted August 7, 2000.)